

Optimized Cancer Cells Sensor Based on 1D Photonic Crystal Vertical Slot Structure

Faiza Bounaas* and Amel Labbani

Abstract—This paper reports the investigation of a one-dimensional (1D) photonic crystal (PhC) sensor with improved performance for detecting different categories of cancer cells. The sensing region consists of a vertical slot (VS) introduced inside the periodic Bragg mirror. The structure operating principle is based on the change of the refractive index (RI) of the analyte incorporated in the VS, which leads to the shift in the resonant wavelength peak. The sensing properties have been numerically simulated and analyzed using the transfer matrix method (TMM). The study shows that the optimization process of the structure tends to enhance sensitivity. From the result of the numerical simulation, it is found that the final optimized sensor exhibits the higher sensitivity of 3201 nm/RIU than other similar devices. We believe that the obtained results will be valuable for designing highly sensitive PhC sensors.

1. INTRODUCTION

The major cause of mortality worldwide is cancer diseases. Cancer can arise from the uncontrolled growth of cells in different parts of the body, so there are more than 100 various types of cancer diseases. The early detection of cancers increases the chances of treating and curing them before they have spread. Therefore, the development of accurate, reliable, and rapid sensors is necessary. The optical biosensor can be utilized for detecting cancerous cells in the early stage.

In recent years, photonic crystals (PhCs) have received great attention in sensing and monitoring applications owing to their advantages of high sensitivity, rapidity, and easy integration. The most important optical characteristic in cancer is refractive index, which mainly determines the difference between normal and malignant cells [1]. The contrast between the refractive indices of the cancerous and normal cells is the principle of photonic biosensors [2–7]. PhCs are artificial optical structures formed by periodic arrays of different materials in one, two, or three dimensions [8, 9]. This periodicity provides a range of frequencies, where the propagation of the electromagnetic waves is forbidden named photonic bandgap (PBG). Making defects in the PhC structure permits modes in the PBG region. The position of the transmission peak is controlled by the change of the refractive index or the shape of the defect. Owing to their interesting feature, PCs have been used in various applications with different designs [10–16].

Recently, one-dimensional photonic crystals have attracted great interest in biosensing and biochemical applications [17–23] due to their high sensitivity, compact size, and their fabrication is possible at any frequency scale compared to 2D and 3D photonic crystals.

In this paper, an optical sensor based on a one-dimensional photonic crystal for detecting five categories of cancer cells (Jurkat, Hela, PC12 MDA-MB-231, and MCF-7) is presented. The optical properties of the designed structure are analyzed using the transfer matrix method (TMM). In our

Received 7 October 2021, Accepted 4 January 2022, Scheduled 6 January 2022

* Corresponding author: Faiza Bounaas (bounaa250@hotmail.fr).

The authors are with the Department of Electronics, Faculty of Science and Technology, University of Mentouri Brothers Constantine 1, Constantine, Algeria.

design, a vertical slot (VS) is used as the sensing medium. To increase the sensitivity of the structure, the presented sensor needs to be optimized. The final optimization device provides very high sensitivity; it reaches 3021 nm/RIU. The results obtained are very satisfactory compared with other similar structures. The design scheme, optimization process, sensing principle, and TMM results are discussed in the following sections.

2. SENSOR DESIGN AND MODELING APPROACH

Our goal of the research is to design an optical sensor based on a one-dimensional photonic crystal capable of detecting different types of cancer cells. The geometric model under study is illustrated in Fig. 1. It is formed of periodic arrays of SiO₂ (A) and TiO₂ (B) with refractive indices n_1 and n_2 , respectively. The period of the perfect structure is $d = d_1 + d_2$, where d_1 and d_2 are the thicknesses of layers A and B, respectively. To study this device for detecting cancer cells, we would introduce a vertical slot (VS) denoted as C in the symmetry center of the structure, which is considered as the sensing medium. All layers are a quarter wavelength ($n_1 d_1 = n_2 d_2 = \lambda_0/4$), in which λ_0 is equal to 1.55 μm . The refractive indices and thicknesses of the PhC utilized in our study are $n_1 = 1.44$, $n_2 = 2.6$, $d_1 = 269.097$ nm, and $d_2 = 149.038$ nm, respectively. As depicted in Fig. 1, the designed system is presented symmetrically as Air/(SiO₂/TiO₂)^V/C/(TiO₂/SiO₂)^V/Air, where V is an integer and represents the number of periods ($V = 13$).

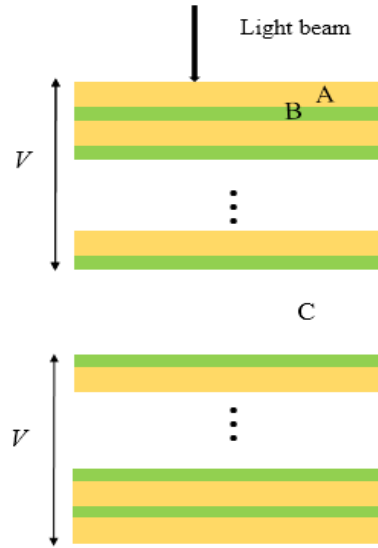


Figure 1. Schematic structure of the Bragg mirror containing a VS.

To analyze the propagation of an optical signal through each layer of the structure, the transfer matrix method is employed. Based on TMM of the second order, the expression for a single layer takes the form [24–26]

$$Q_i = \begin{bmatrix} \cos d_i Q_i & \left(-\frac{i}{P_i}\right) \sin d_i Q_i \\ -iP_i \sin d_i Q_i & \cos d_i Q_i \end{bmatrix} \quad (1)$$

$$Q_i = \frac{\omega}{c} n_i \cos \theta_i \quad (2)$$

where d_i is the layer thickness.

The full transfer matrix of the 1D PhC is presented by the product of all single layering transfer matrices, shown as:

$$Q_T = (Q_A Q_B)^V Q_C (Q_B Q_A)^V \quad (3)$$

where V is the number of binary layers in the Bragg mirrors, and Q_C is the transfer matrix of the vertical slot. The transmission coefficient for the defective 1D photonic crystal is expressed as follows:

$$t = \left| \frac{2P_0}{(Q_{11} + Q_{12}P_0)P_0 + Q_{21} + Q_{22}P_0} \right|^2 \quad (4)$$

3. NON-OPTIMIZED SENSOR DESIGN

In this section, we discuss the optical properties of the proposed sensor. The transfer matrix method is utilized to calculate the transmittance and resonant defect shift of the device at normal incidence. The numerical results show that the presented structure without any defects possesses one PBG in the range of 1302.9 nm–1894.6 nm. As shown in Fig. 2, the PBG is relatively wide enough to meet the sensing demand where the transmission peak generates a large frequency shift. Initially, a normal cell with a refractive index $n = 1.35$ has been infiltrated into the vertical slot. As shown in Fig. 3, one narrow resonant peak is generated inside the PBG. This derived peak is a result of the localization of light inside the defect. Its position is located at 1534.525 nm, with an intensity of 99.5%. Thus, strong confinement of the optical field within the vertical slot is obtained. The thickness of the VS is assumed to be equal to 1700 nm. It can also be noted that the signal response outside the gap Bragg is affected by some fluctuation. This is due to the existence of the defect inside the structure. When different categories of cancer cells with known refractive indices (Table 1) are filled into the VS, the resonant wavelength moves to a new position. Fig. 4 is a plot illustrating the shift of the transmission peak. From the figure, we can observe that the resonant mode travels to longer wavelength regions from 1534.525 nm to 1575.833 nm when RI varies from 1.35 (Normal cell) to 1.401 (MCF-7 cancer). This explains that the structure provides a more high-dielectric region inside the vertical slot.

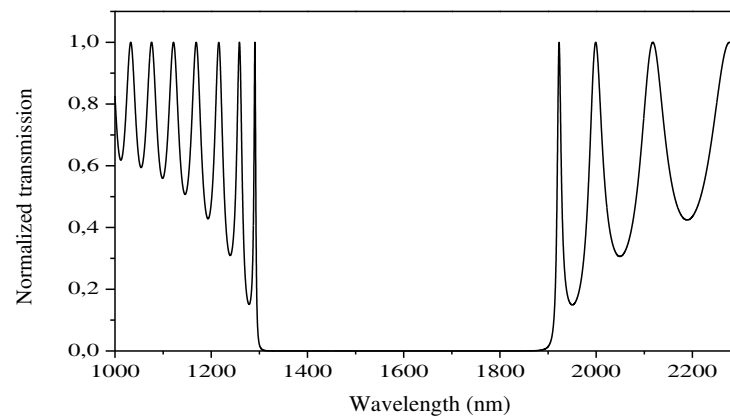


Figure 2. The transmission spectra of the basic structure 1D photonic crystal at normal incidence.

Table 1. The refractive index of the used cancerous cells [27].

Cell	Refractive index (RIU)
Normal cell	1.35
Jurkat	1.39
Hela	1.392
PC 12	1.395
MDA-MB-231	1.399
MCF-7	1.401

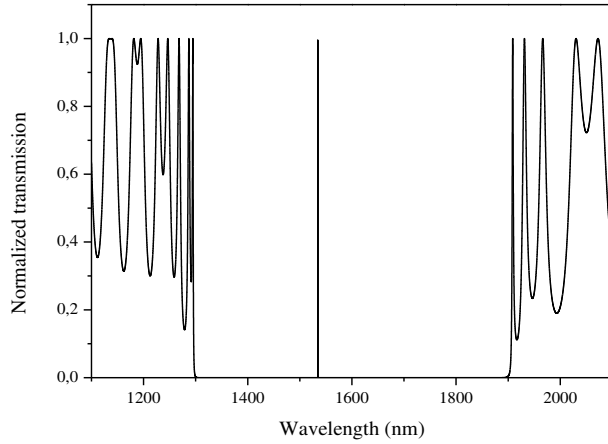


Figure 3. The transmission spectra of the proposed sensor in the presence of normal cells in VS.

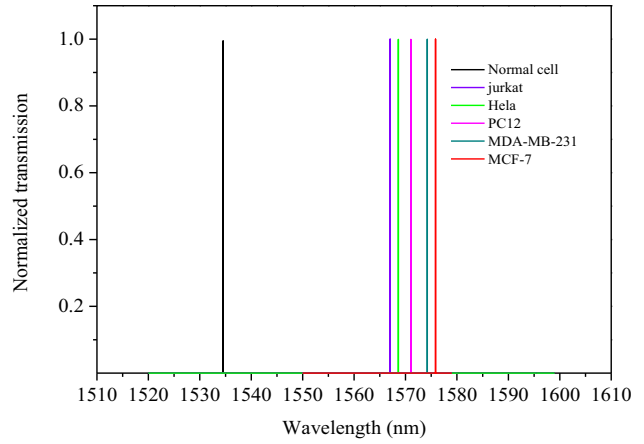


Figure 4. The transmission spectra of the proposed sensor in the presence of different categories of cancerous cells in VS.

The most significant parameter utilized to evaluate the performance of the sensor is called the sensitivity (S), and it is expressed as:

$$S = \frac{\Delta\lambda}{\Delta n} \tag{5}$$

where $\Delta\lambda$ represents the wavelength shifting caused by the shift of the refractive index and is calculated in terms of nm/RIU. According to our simulation results, the designed structure sensitivity is equal to 812.025 nm/RIU.

The variation tendency of the sensitivity and the resonant wavelength shift with the change of the refractive index is plotted in Fig. 5. As seen in this figure, the sensitivity decreases linearly towards 809.96 nm/RIU when RI varies from 1.35 to 1.401. In contrast, the displacement of the mode becomes larger when RI augments. It can also be noted that the transmission efficiency is unaffected and equal to unity.

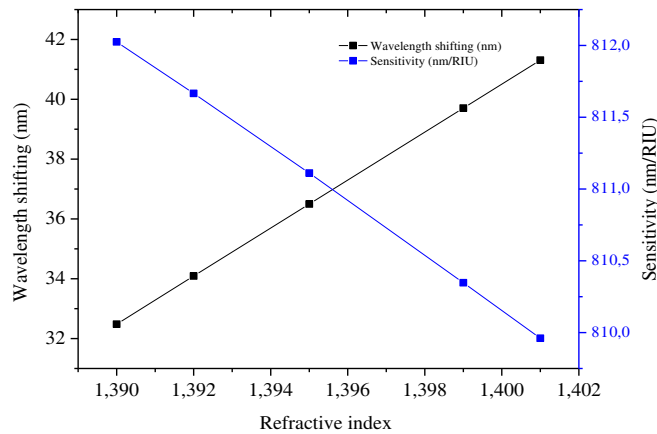


Figure 5. Wavelength shift and sensitivity as a function of the refractive index variation.

4. OPTIMIZED SENSOR DESIGN

In this part, we focus our objective on the optimization of the previous sensor to improve the detection sensitivity of the structure. For the optimization process, we use two steps: Firstly, we surround the

sensing region with a composite material. Secondly, we place a prism on the front of the structure and vary the incident angle (θ).

4.1. Effect of the Filling Factor f on the Sensitivity

In this section, the previous sensor is optimized by modifying the design of the structure in such a way that the sensitivity is improved. The optimization is done by removing two layers situated on each side of the VS and replacing them with composite material formed by Ag nanoparticles (Ag NP) dispersed in the TiO_2 matrix. A schematic of the modified structure is illustrated in Fig. 6. To describe the dielectric permittivity $\tilde{\varepsilon}(\omega)$ of the obtained composite material (Ag + TiO_2), we use the Maxwell-Garnett formula, which is widely utilized in the analysis of composite media that contain various kinds of small particles inclusions [28]

$$\frac{\tilde{\varepsilon}(\omega) - \varepsilon_m}{\tilde{\varepsilon}(\omega) + 2\varepsilon_m} = f \frac{\varepsilon_n - \varepsilon_m}{\varepsilon_n + 2\varepsilon_m} \tag{6}$$

where ε_m is the dielectric permittivity of TiO_2 matrix; f is the volume fraction occupied by Ag nanoparticles; ω is the radiation frequency; ε_n is the dielectric permittivity of the silver nanoparticles and is obtained from a modified Drude model which has the following form [29, 30]:

$$\varepsilon_n(\omega) = \varepsilon_a - \frac{\omega_p^2}{\omega(\omega + i\gamma)} \tag{7}$$

where $\varepsilon_a = 5.45$, ω_p is the plasma frequency ($\omega_p = 1.72 \times 10^{16}$ rad/s) [29], and γ is the plasma damping constant, which represents a size-dependent function for metallic nanoparticles of spherical shape and can be written as [29]:

$$\gamma = \frac{v^F}{l} + \frac{v^F}{r} \tag{8}$$

where $v^F = 138 \times 10^6$ m/s (Fermi velocity), $l = 52$ nm (electron mean free path at room temperature), and $2r = d$ with d being the silver Ag NP diameter. From Eqs. (6) and (7), we can deduce the real and imaginary parts of the composite material:

$$\varepsilon_m(\omega) = \varepsilon'_m(\omega) + i\varepsilon''_m(\omega) \tag{9}$$

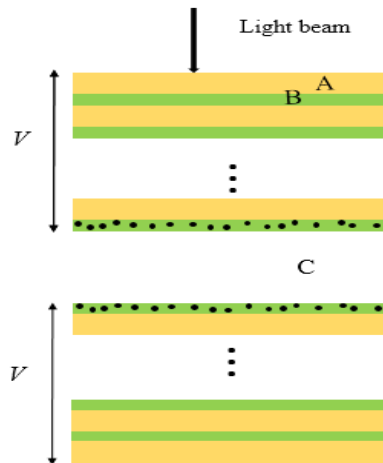


Figure 6. Schematic structure of the Bragg mirror containing a VS surrounded by composite material.

We have plotted the real part of the dielectric permittivity in Fig. 7(a) and the imaginary part in Fig. 7(b) as a function of f , for $r = 1, 2$ and 5 nm, where r is the radius of the Ag aggregates. It can be seen from Fig. 7(a) that ε'_m augments as the filling factor increases, but remains nearly invariant

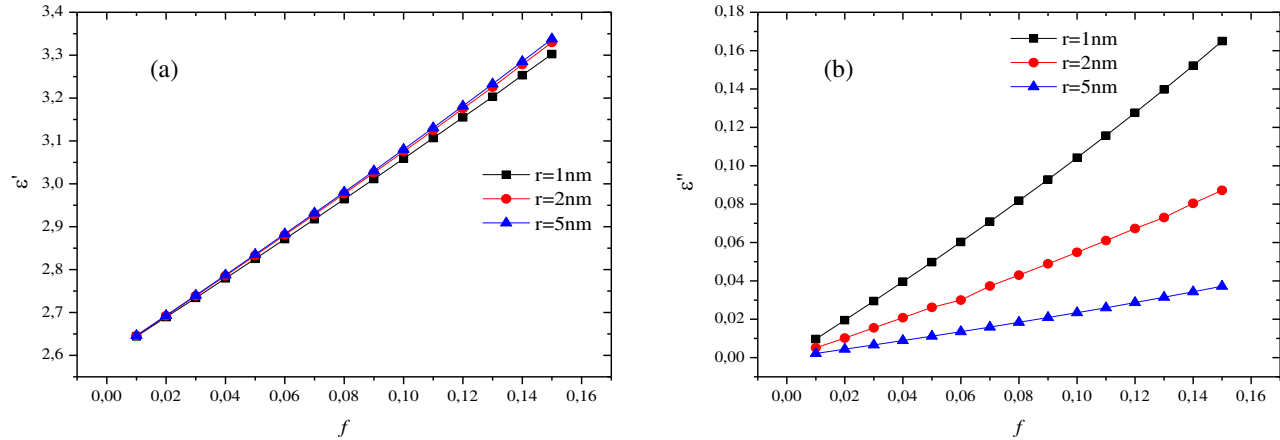


Figure 7. (a) Real part and (b) imaginary part of the optical permittivity of the composite material as a function of the filling factor for $r = 1$ nm, 2 nm, and 5 nm.

with the increase in r . The significant increase of ϵ'_m is due to the presence of Ag NP in the matrix. Similarly, the imaginary part of $\tilde{\epsilon}(\omega)$ is affected by the volume fraction f and the radius r of the metal. As shown in Fig. 7(b), ϵ''_m increases when f varies from 1% to 15% and decreases when r increases. The increase of ϵ''_m implies that the composite material will absorb the optic wave passing through its region. For this reason, we have chosen $r = 5$ nm as the size of rod radius in all the following studies. To further investigate the effect of the filling factor on the sensor performance, we have plotted the sensitivity versus f at normal incidence.

Figure 8 represents the relationship between S and the filling factor for five kinds of cancer cells. It shows that the sensor sensitivity increases when f augments. The results reveal that the maximum values of S obtained at $f = 4\%$ for MCF-7, MDA-MB-231, PC12, HeLa, and Jurkat are 840.49 nm/RIU, 840.816 nm/RIU, 841.444 nm/RIU, 841.9047 nm/RIU, and 842.25 nm/RIU, respectively, which seems a good result compared to the non-optimized structure. This significant increase is due to the strong shift of the resonant wavelength peak. Fig. 9 demonstrates that the transmission peak moves from 1547.625 nm to 1590.49 nm when n_c of the VS varies from 1.35 (normal cell) to 1.401 (MCF-7). In addition, it can be noticed that the intensity of the resonant peak is reduced and attains 78% when $f = 4\%$. This lower transmission efficiency is due to the lossless feature of the composite material.

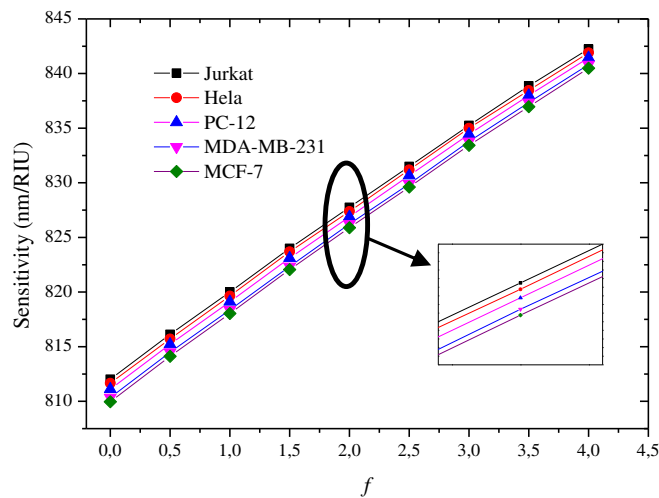


Figure 8. The sensitivity of the sensor as a function of the volume fraction f for different cancer cells.

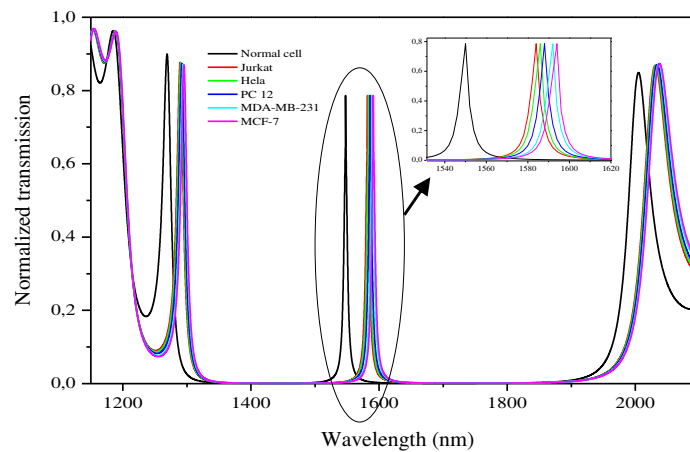


Figure 9. The transmission spectra of the sensor in the presence of different categories of cancerous cells in VS at $f = 4\%$.

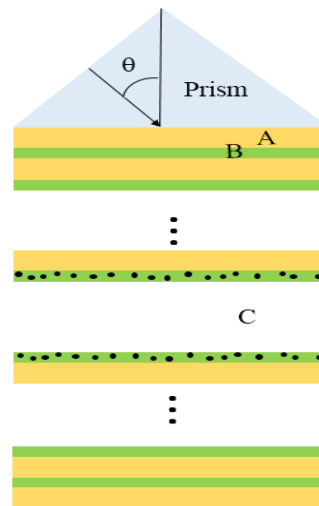


Figure 10. The schematic diagram of the optimized structure.

4.2. Effect of the Prism and Angle of Incidence on the Sensitivity

Our optimization is not limited to doping the two neighboring layers of the VS, but it will be extended by adding a prism to the structure and varying the angle of incidence. To do so, we kept the same device presented in Section 4.1 and attached a prism in front of the structure. The filling factor and refractive index of the prism used in this section are 4% and $n_p = 1.6$, respectively. The schematic presentation of the new optimized device is shown in Fig. 10. To analyze the effect of the incident angle (θ) on the resonant peak, we vary θ from 0° to 50° . The simulation results show clearly that the resonant mode is influenced by the change of θ . We also recorded that by increasing θ the peak of each type of cancer cells shifted towards lower wavelengths. In addition, we plotted S as a function of θ for two cases: with and without attaching prism, which gave us information about the sensibility of the sensor. It is clear from Fig. 11 that for θ more than 25° , the sensitivity of the Jurkat cancer cell of the first case (with attached prism) improves significantly and gains the maximum value of 3201 nm/RIU when $\theta = 50^\circ$. To further investigate the effect of the prism on the sensitivity, we have plotted the normalized transmission spectra of the optimized structure at incidence angle 50° for different cancer cells. The results are presented in Fig. 12, and the inset shows the amplified image of all the transmission peaks. The detail of the calculated λ , $\Delta\lambda$, and S are given in Table 2. In summary, one can say that the

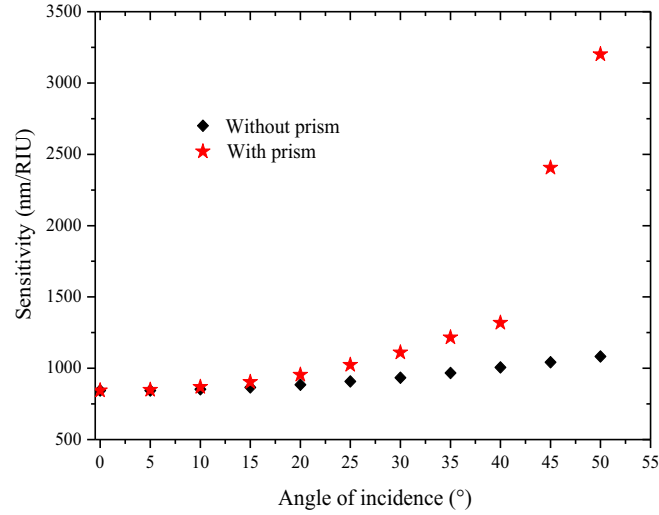


Figure 11. Sensitivity of the optimized sensor versus θ .

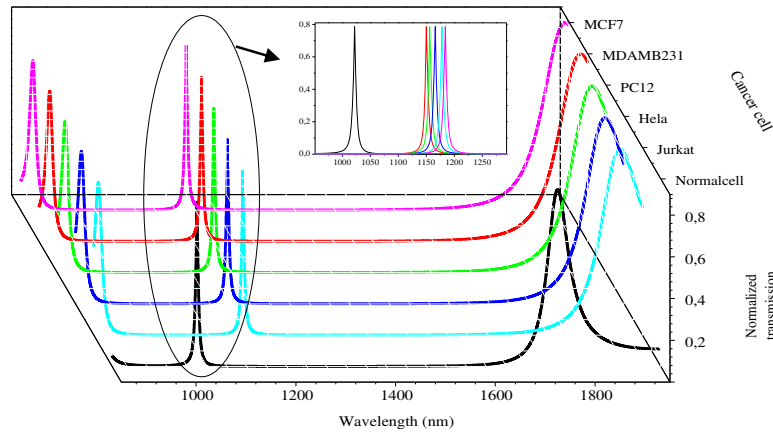


Figure 12. Transmission spectra of 1D PhC at $\theta = 50^\circ$ and $f = 4\%$ for different cancer cells.

optimized structure is most sensitive for HeLa cancer cells and is enhanced by about more than three orders magnitude better than the previous one reported in Section 4.1, which can be considered as an important improvement. In addition, the numerical simulations illustrate that our presented structure gives better performance than other proposed sensors with other designs. The comparison of our results with some recent works is summarized in Table 3. In summary, we believe that the obtained results render our device suitable for detecting different cancer cells.

Table 2. Resonant mode, wavelength shifting and sensitivity with different types of cancer cells.

Cancerous cell	λ (nm)	$\Delta\lambda$	S (nm/RIU)
Normal cell	1020.2	/	/
Jurkat	1148.04	128.04	3201
HeLa	1154.66	134.46	3201.42
PC 12	1164.03	143.83	3196.22
MDA-MB-231	1176	155.8	3179.59
MCF-7	1181.94	161.74	2741.35

Table 3. Comparison of the results with other reported works.

Sensor structure	Maximum sensitivity (nm/RIU)	Reference
Cavity surrounded by Thin graphene layer in 1D-PhC	560.25	[31]
One-dimensional PhC cavity	74.50	[32]
One-dimensional PhC cavity	2175	[33]
One-dimensional PhC nano composite material coated 1D-PhC	43.13	[34]
2D photonic crystal waveguide	2360.12	[35]
Resonator coupled waveguide (2.5 PhC)	720	[2]
Nanocavity coupled photonic crystal waveguide (2.5 PhC)	391.7	[36]
1D-PhC vertical slot structure	3201	This work

5. CONCLUSION

In this work, a highly sensitive cancer cells sensor based on a 1D-PhC platform is investigated. The sensing region consists of a vertical slot (VS) introduced inside the periodic Bragg mirror. The structure operating principle is based on the change of the refractive index (RI) of the analyte incorporated in the VS, which leads to the shift in the resonant wavelength peak. The sensing properties have been numerically simulated and analyzed using the transfer matrix method (TMM). The study shows that the optimization process of the structure tends to enhance sensitivity. From the numerical simulation result, it is found that the final optimized sensor exhibits the higher sensitivity of 3201 nm/RIU than other similarly designed devices. We believe that the obtained results will be valuable for designing highly sensitive PhC cancer cells sensors.

REFERENCES

- Liu, P. Y., L. K. Chin, W. Ser, H. F. Chen, C.-M. Hsieh, C.-H. Lee, K.-B. Sung, T. C. Ayi, P. H. Yap, and B. Liedberg, "Cell refractive index for cell biology and disease diagnosis: Past, present and future," *Lab on a Chip*, Vol. 16, No. 4, 634–644, 2016.
- Danaie, M. and B. Kiani, "Design of a label-free photonic crystal refractive index sensor for biomedical applications," *Photonics and Nanostructures — Fundamentals and Applications*, Vol. 31, 89–98, 2018.
- Ayyanar, N., G. Thavasi Raja, M. Sharma, and D. Sriram Kumar, "Photonic crystal fiber-based refractive index sensor for early detection of cancer," *IEEE Sensors J.*, Vol. 18, No. 17, 7093–7099, 2018.
- Roy, S. K. and P. Sharan, "Photonic crystal based sensor for DNA analysis of cancer detection," *Silicon Photonics & High Performance Computing*, Vol. 718, 79–85, 2018.
- Emami Nejad, H., A. Mir, and A. Farmani, "Supersensitive and tunable nano-biosensor for cancer detection," *IEEE Sensors J.*, Vol. 19, No. 13, 4874–4881, 2019.
- Parvin, T., K. Ahmed, A. M. Alatwi, and A. N. Z. Rashed, "Differential optical absorption spectroscopy-based refractive index sensor for cancer cell detection," *Optical Review*, Vol. 28, No. 01, 134–143, 2021.
- Segovia-Chaves, F. and H. Vinck-Posada, "Superconductor-semiconductor one-dimensional photonic crystal using a cancer cell as a defect layer," *Optik*, Vol. 224, 165465, 2020.

8. Yablonovitch, E., "Inhibited spontaneous emission in solid-state physics and electronics," *Physical Review Letters*, Vol. 58, No. 20, 2059–2062, 1987.
9. John, S., "Strong localization of photons in certain disordered dielectric superlattices," *Physical Review Letters*, Vol. 58, No. 23, 2486–2489, 1987.
10. Bounaas, F. and A. Labbani, "High sensitivity temperature sensor based on photonic crystal resonant cavity," *Progress In Electromagnetics Research Letters*, Vol. 90, 85–90, 2020.
11. Hosseinzadeh Sani, M., A. Ghanbari, and H. Saghaei, "An ultra-narrowband all-optical filter based on the resonant cavities in rod-based photonic crystal microstructure," *Opt. Quant. Electron.*, Vol. 52, No. 6, 295, 2020.
12. Moumeni, I. and A. Labbani, "Very high efficient of 1×2 , 1×4 and 1×8 Y beam splitters based on photonic crystal ring slot cavity," *Opt. Quant. Electron.*, Vol. 53, No. 2, 129, 2021.
13. Sana, A. K., K. Honzawa, Y. Amemiya, and S. Yokoyama, "Silicon photonic crystal resonators for label free biosensor," *Japanese Journal of Applied Physics*, Vol. 55, No. 45, 04EM11, 2016.
14. Pitruzzello, G. and T. F. Krauss, "Photonic crystal resonances for sensing and imaging," *Journal of Optics*, Vol. 20, No. 07, 073004, 2018.
15. Abirami, N. and K. S. Joseph Wilson, "Investigation on photonic band gap of a magneto photonic crystal," *Optik*, Vol. 208, 164092, 2020.
16. Naghizade, S. and H. Saghaei, "A novel design of all-optical 4 to 2 encoder with multiple defects in silica-based photonic crystal fiber," *Optik*, Vol. 222, 165419, 2020.
17. Ankita, B. S. and A. Bhargava, "Biosensor application of one-dimensional photonic crystal for malaria diagnosis," *Plasmonics*, Vol. 16, No. 01, 59–63, 2021.
18. Aly, A. H., Z. A. Zaky, A. S. Shalaby, A. M. Ahmed, and D. Vigneswaran, "Theoretical study of hybrid multifunctional one-dimensional photonic crystal as a flexible blood sugar sensor," *Physica Scripta*, Vol. 95, No. 03, 035510, 2020.
19. Mehaney, A., "Phononic crystal as a neutron detector," *Ultrasonics*, Vol. 93, 37–42, 2019.
20. Segovia-Chaves, F., "Transmittance spectrum of a defective one-dimensional photonic crystal with a protein solution," *Optik*, Vol. 231, 166408, 2021.
21. Zaky, Z. A., A. M. Ahmed, A.S . Shalaby, and A. H. Aly, "Refractive index gas sensor based on the Tamm state in a one-dimensional photonic crystal: Theoretical optimization," *Scientific Reports*, Vol. 10, No. 01, 1–9, 2020.
22. Ramanujam, N. R., S. K. Patel, N. Manohar Reddy, S. A. Taya, D. Vigneswaran, and M. S. Mani Rajan, "One-dimensional ring mirror-defect photonic crystal for detection of mycobacterium tuberculosis bacteria," *Optik*, Vol. 219, 165097, 2020.
23. Habli, O., Y. Bouazzi, and M. Kanzari, "Gas sensing using one-dimensional photonic crystal nanoresonators," *Progress In Electromagnetics Research C*, Vol. 92, 251–263, 2019.
24. Lee, C.-M. and Y. Xu, "A modified transfer matrix method for prediction of transmission loss of multilayer acoustic materials," *Journal of Sound and Vibration*, Vol. 326, Nos. 1–2, 290–301, 2009.
25. Fan, C., J. Wang, S. Zhu, J. He, P. Ding, and E. Liang, "Optical properties in one-dimensional graded soft photonic crystals with ferrofluids," *Journal of Optics*, Vol. 15, No. 5, 055103, 2013.
26. Yeh, P., *Optical Waves in Layered Media*, Vol. 95, Wiley, New York, 1988.
27. Liang, X. J., A. Q. Liu, C. S. Lim, T. C. Ayi, and P. H. Yap, "Determining refractive index of single living cell using an integrated microchip," *Sensors and Actuators A: Physical*, Vol. 133, No. 02, 349–354, 2007.
28. Ramanujam, N. R. and K. S. J. Wilson, "Optical properties of silver nanocomposites and photonic band gap — Pressure dependence," *Optics Communications*, Vol. 368, 174–179, 2016.
29. Segovia-Chaves, F., H. A. Elsayed, A. Mehaney, and A. M. Ahmed, "Defect mode modulation for a protein solution cavity surrounded by graphene and nanocomposite layers," *Optik*, Vol. 242, 167161, 2021.
30. Kok, M. H., R. Ma, J. C. W. Lee, W. Y. Tam, C. T. Chan, P. Sheng, and K. W. Cheah, "Photonic band gap effect and structural color from silver nanoparticle gelatin emulsion," *Physical Review E*, Vol. 72, No. 4, 047601, 2005.

31. Segovia-Chaves, F. and J. C. Trujillo Yague, "Sensitivity optimization of cells immersed in a cavity surrounded by thin graphene layers in one-dimensional photonic crystals," *Optik*, Vol. 231, 166355, 2021.
32. Bijalwan, A., B. K. Singh, and V. Rastogi, "Analysis of one-dimensional photonic crystal based sensor for detection of blood plasma and cancer cells," *Optik*, Vol. 226, 165994, 2021.
33. Aly, A. H. and Z. A. Zaky, "Ultra-sensitive photonic crystal cancer cells sensor with a high-quality factor," *Cryogenics*, Vol. 104, 102991, 2019.
34. Ramanujam, N. R., I. S. Amiri, S. A. Taya, S. Olyaei, R. Udaiyakumar, A. P. Pandian, K. J. Wilson, P. Mahalakshmi, and P. P. Yupapin, "Enhanced sensitivity of cancer cell using one dimensional nano composite material coated photonic crystal," *Microsystem Technologies*, Vol. 25, No. 1, 189–196, 2019.
35. Panda, A. and P. Puspa Devi, "Photonic crystal biosensor for refractive index based cancerous cell detection," *Optical Fiber Technology*, Vol. 54, 102123, 2020.
36. Jindal, S., S. Sobti, M. Kumar, S. Sharma, and M. K. Pal, "Nanocavity-coupled photonic crystal waveguide as highly sensitive platform for cancer detection," *IEEE Sensors J.*, Vol. 16, 3705–3710, 2016.